

# Distribution Distillation Loss: Generic Approach for Improving Face Recognition from Hard Samples

Yuge Huang<sup>†\*</sup> Pengcheng Shen<sup>†\*</sup> Ying Tai<sup>‡#</sup> Shaoxin Li<sup>‡#</sup> Xiaoming Liu<sup>‡</sup>

Jilin Li<sup>†</sup> Feiyue Huang<sup>†</sup> Rongrong Ji<sup>§</sup>

<sup>†</sup>Youtu Lab, Tencent <sup>‡</sup>Michigan State University <sup>§</sup>Xiamen University

<sup>†</sup>{yugehuang, quantshen, yingtai, darwinli, jerolinli, garyhuang}@tencent.com

<sup>‡</sup>liuxm@cse.msu.edu, <sup>§</sup>rrji@xmu.edu.cn

## Abstract

Large facial variations are the main challenge in face recognition. To this end, previous variation-specific methods make full use of task-related prior to design special network losses, which are typically not general among different tasks and scenarios. In contrast, the existing generic methods focus on improving the feature discriminability to minimize the intra-class distance while maximizing the inter-class distance, which perform well on easy samples but fail on hard samples. To improve the performance on those hard samples for general tasks, we propose a novel Distribution Distillation Loss to narrow the performance gap between easy and hard samples, which is a simple, effective and generic for various types of facial variations. Specifically, we first adopt state-of-the-art classifiers such as ArcFace to construct two similarity distributions: teacher distribution from easy samples and student distribution from hard samples. Then, we propose a novel distribution-driven loss to constrain the student distribution to approximate the teacher distribution, which thus leads to smaller overlap between the positive and negative pairs in the student distribution. We have conducted extensive experiments on both generic large-scale face benchmarks and benchmarks with diverse variations on race, resolution and pose. The quantitative results demonstrate the superiority of our method over strong baselines, e.g., Arcface and Cosface.

## 1. Introduction

A primary challenge of large-scale face recognition on unconstrained imagery is to handle the diverse variations on pose, resolution, race, age and illumination, *etc.* While some variations are easy to address, many others are relatively difficult. As shown in Fig. 1, images with small varia-

\* indicates equal contributions. # denotes Ying Tai and Shaoxin Li are corresponding authors. Code will be publicly available upon publication.

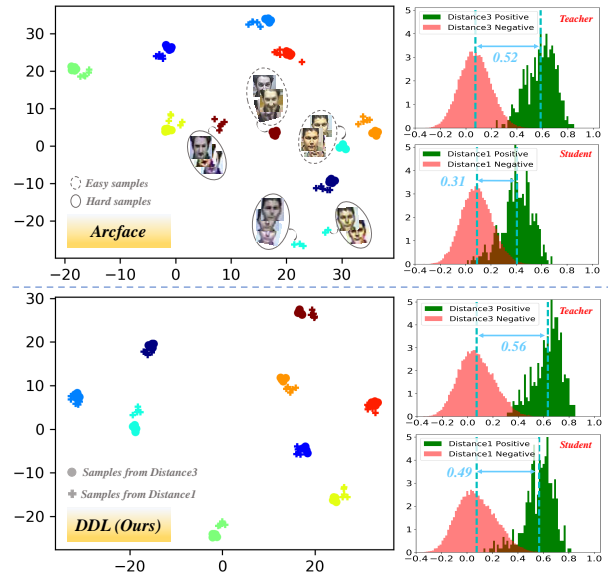


Figure 1: Comparisons with Arcface [5] on SCface [9] dataset. **Left:** T-SNE [19] visualizations on features, where the same color indicates samples of the same subject. Distance1 ( $d_1$ ) and Distance3 ( $d_3$ ) indicate images were captured at distances of 4.2 and 1.0m, respectively. **Right:** Cosine similarity distributions of both methods. Each method has two distributions from  $d_3$  and  $d_1$ , where there are also two distributions from the positive and negative pairs with a margin indicating the difference of their expectations. With our distribution distillation loss between the teacher and student distributions, our method effectively narrows the performance gap between the easy and hard samples, decreasing the expectation margin from **0.21** (0.52-0.31) to **0.07** (0.56-0.49).

tions can be well addressed by the State-of-the-Art (SOTA) facial classifier like ArcFace [5] and tightly group in the feature space, which we denote as the *easy samples*. In contrast, images with large variations are more difficult to tackle and usually far away from the easy ones, which we denote as the *hard samples*. To better recognize these hard samples, there are usually two schemes: *variation-specific*

methods and *generic* methods.

Variation-specific methods are usually designed for a specific task. For instance, to achieve pose-invariant face recognition, either handcrafted or learned features are extracted, which are able to enhance robustness against pose while remaining discriminative to the identities [32]. Recently, joint face frontalization and disentangled identity preservation are incorporated to facilitate the pose-invariant feature learning [34, 51]. To address resolution-invariant face recognition, a unified feature space is learned in [14, 26] for mapping Low-Resolution (LR) and High-Resolution (HR) images. The works [3, 53] first apply super-resolution on the LR images and then perform recognition on the super-resolved images. However, the above methods are specifically designed for the respective variations, therefore their ability to generalize from one variation to another is limited. Yet, it is highly desirable to handle multiple variations in real world recognition systems.

Different from variation-specific methods, generic methods focus on improving the discriminate power of facial features, for small intra-class and large inter-class distances. Basically, the prior works fall into two categories, *i.e.*, softmax loss-based and triplet loss-based methods. Softmax loss-based methods regard each identity as a unique class to train the classification networks. Since the traditional softmax loss is insufficient to acquire the discriminate features, several variants [5, 16, 38, 42] are proposed to enhance the discriminability. In contrast, triplet loss-based methods [21, 24] directly learn an Euclidean space embedding for each face, in which faces from the same person are closer, forming separated cluster to faces of other persons. With large-scale training data and well-designed network structures, both types of methods can obtain promising results.

However, the performance of these methods degrades dramatically on hard samples, such as very large-pose and low-resolution faces. As illustrated in Fig. 1, the features extracted from HR images (*i.e.*,  $d_3$ ) by the strong face classifier of Arcface [5] are well separated, but the features extracted from LR images (*i.e.*,  $d_1$ ) cannot be well distinguished. From the perspective of the angle distributions of positive and negative pairs, we can easily observe that Arcface generates more confusion regions on LR face images. It is thereby a natural consequence that such generic methods perform worse on hard samples.

To narrow the performance gap between the easy and hard samples, we propose a novel Distribution Distillation Loss (DDL). By leveraging the best of both the *variation-specific* and *generic* methods, our method is generic and can be applied to diverse variations to improve face recognition in hard samples. Specifically, we first adopt current SOTA face classifiers as the baseline (*e.g.*, Arcface) to construct the initial similarity distributions between teacher (*e.g.*, easy samples from  $d_3$  in Fig. 1) and student (*e.g.*, hard samples

from  $d_1$  in Fig. 1) according to the difficulties of samples, respectively. Compared to finetuning the baseline models with domain data, our method firstly does not require extra data or inference time (*i.e.*, *simple*); secondly makes full use of hard sample mining and directly optimizes the similarity distributions to improve the performance on hard samples (*i.e.*, *effective*); and finally can be easily applied to address different kinds of large variations (*i.e.*, *general*).

To sum up, the contributions of this work are three-folds:

- Our method narrows the performance gap between easy and hard samples on *diverse* facial variations, which is simple, effective and general.
- To our best knowledge, it is the first work that adopts similarity distribution distillation loss for face recognition, which provides a new perspective to obtain more discriminative features to better address hard samples.
- Significant gains compared to the SOTA Arcface classifier are reported, *e.g.*, 97.0% over 92.7% on SC-face [9], 93.4% over 92.1% on CPLFW [58], 90.7% over 89.9% (@FAR=1e-4) on IJB-B [43] and 93.1% over 92.1% (@FAR=1e-4) on IJB-C [20].

## 2. Related Work

**Loss Function in FR.** Loss function design is pivotal for large-scale face recognition. Softmax is commonly used for face recognition [29, 33, 37], which encourages the separability of features but the learned features are not guaranteed to be discriminative. To address this issue, contrastive [28] and triplet [21, 24] losses are proposed to increase the margin in the Euclidean space. However, both contrastive and triplet losses occasionally encounter training instability due to the selection of effective training samples. As a simple alternative, center loss and its variants [6, 42, 55] are proposed to compress the intra-class variance. More recently, angular margin-based losses [5, 16, 17, 36] facilitate feature discrimination, and thus lead to larger angular/cosine separability between learned features. The above loss functions are designed to apply constraints either between samples, or between sample and center of the corresponding subject.

In contrast, our proposed loss is *distribution* driven. While being similar to the histogram loss [35] that constrains the overlap between the distributions of positive and negative pairs across the training set, our loss differs in that we first separate the training set to a teacher distribution (easy samples) and student distribution (hard samples), and then constrain the student distribution to approximate the teacher distribution via our novel loss, which narrows the performance gap between easy and hard samples.

**Variation-Specific FR.** Apart from those generic solutions [29, 33] for face recognition, there are also many methods designed to handle specific facial variations, such as resolutions, poses, illuminations, expressions and occlusions.

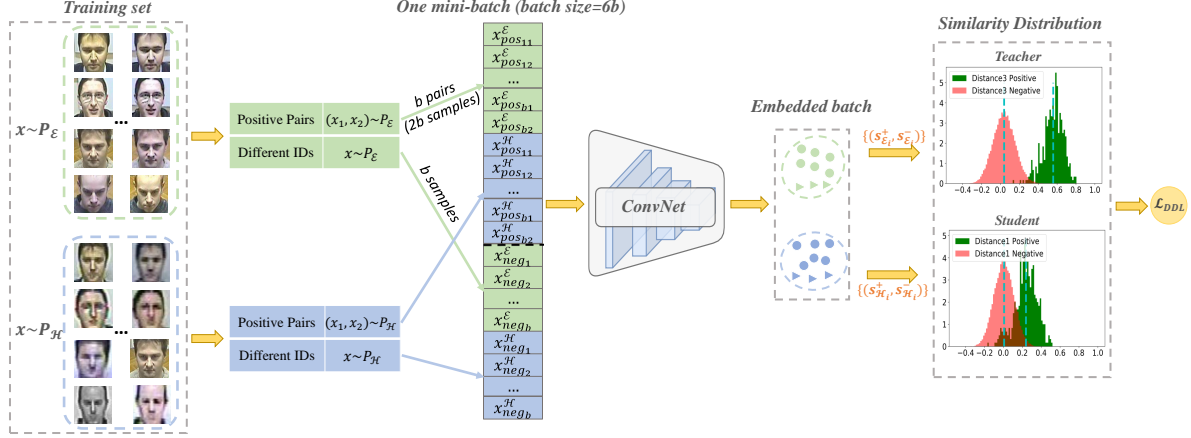


Figure 2: **Illustration of our DDL.** We sample  $b$  positive pairs (*i.e.*,  $2b$  samples) and  $b$  samples with different identities, for both of teacher  $P_E$  and student  $P_H$  distributions, to form one mini-batch.  $\{(s_{E_i}^+, s_{E_i}^-) | i = 1, \dots, b\}$  indicates we construct  $b$  positive and negative pairs from  $P_E$  via Eqs. 1 and 2 respectively to estimate the teacher distribution. And  $\{(s_{H_i}^+, s_{H_i}^-) | i = 1, \dots, b\}$  also indicates we construct  $b$  positive and negative pairs from  $P_H$  via Eqs. 1 and 2 respectively to estimate the student distribution.

For example, cross-pose FR [32, 34, 50, 57] is very challenging, and previous methods mainly focus on either face frontalization or pose invariant representations. Low resolution FR is also a difficult task, especially in the surveillance scenario. One common approach is to learn a unified feature space for LR and HR images [10, 18, 59]. And the other way is to perform super resolution [3, 30, 31, 53] to enhance the facial identity information. Differing from the above methods that mainly deal with one specific variation, our novel loss is a generic approach to improve FR from hard samples, which is applicable to a wide variety of variations.

**Knowledge Distillation.** Knowledge Distillation (KD) is an emerging topic. Its basic idea is to distill knowledge from a large teacher model into a small one by learning the class distributions provided by the teacher via softened softmax [11]. Typically, Kullback Leibler (KL) divergence [11, 56] and Maximum Mean Discrepancy (MMD) [13] can be adopted to minimize the posterior probabilities between teacher and student models. More recently, Generative Adversarial Networks [8] are introduced as an alternative way to learn the true data distribution [41, 47]. Our distillation loss differs from the above conventional KD methods in two aspects: 1) The conventional KD methods adopt different teacher (*i.e.*, high-capacity) and student models, while ours use the same model to construct different teacher (*i.e.*, easy samples) and student (*i.e.*, hard samples) distributions. 2) The objective of many KD methods is for model compression, while ours is generic to improve the recognition performance from hard samples.

### 3. The Proposed Method

Fig. 2 illustrates the framework of the proposed method. We separate the training set into two parts, *i.e.*,  $\mathcal{E}$  for easy samples and  $\mathcal{H}$  for hard samples to form the teacher and stu-

dent distributions, respectively. In general, for each mini-batch during training, we sample from both parts. To ensure a good teacher distribution, we use the SOTA FR model [5] as our initialization. The extracted features are used to construct the positive and negative pairs (Sec. 3.1), which are further utilized to estimate the similarity distributions (Sec. 3.2). Finally, based on the similarity distributions, the proposed DDL is kicked in to train the classifier (Sec. 3.3).

#### 3.1. Sampling Strategy from $P_E$ and $P_H$

First, we introduce the details on how we construct the positive and negative pairs in one mini-batch during training. Given two types of input data from both  $P_E$  and  $P_H$ , each mini-batch consists of four parts, two kinds of positive pairs (*i.e.*,  $(x_1, x_2) \sim P_E$  and  $(x_1, x_2) \sim P_H$ ), and two kinds of samples with different identities (*i.e.*,  $x \sim P_E$  and  $x \sim P_H$ ). To be specific, we on one hand construct  $b$  positive pairs (*i.e.*,  $2b$  samples), and on the other hand  $b$  samples with different identities from  $P_E$  and  $P_H$ , respectively. As the result, there are  $6b = (2b + b) * 2$  samples in each mini-batch (see Fig. 2 for more details).

**Positive Pairs.** The positive pairs are constructed offline in advance, and each pair consist of two samples with the same identity. As shown in Fig. 2, samples of each positive pair are arranged in order. After emebdding data into a high-dimensional feature space by a deep network  $\mathcal{F}$ , the similarity of a positive pair  $s^+$  can be obtained as follows:

$$s_i^+ = \langle \mathcal{F}(x_{pos_{i1}}), \mathcal{F}(x_{pos_{i2}}) \rangle, i = 1, \dots, b \quad (1)$$

where  $x_{pos_{i1}}, x_{pos_{i2}}$  are the samples of one positive pair. Note that positive pairs with similarity less than 0 are usually outliers, which are deleted as a practical setting since our main goal is not to specifically handle noise.

**Negative Pairs.** Different from the positive pair, we construct negative pairs online from the samples with different

identities via hard negative mining, which selects negative pairs with the largest similarities. To be specific, the similarity of a negative pair  $s^-$  is defined as:

$$s_i^- = \max_j \left( \{s_{ij}^- = \langle \mathcal{F}(x_{neg_i}), \mathcal{F}(x_{neg_j}) \rangle > | j = 1, \dots, b\} \right), \quad (2)$$

where  $x_{neg_i}, x_{neg_j}$  are from different subjects. Once the similarities of positive and negative pairs are constructed, the corresponding distributions can be estimated, which is described in the next subsection.

### 3.2. Similarity Distribution Estimation

The process of similarity distribution estimation is similar to [35], which is performed in a simple and piece-wise differentiable manner using 1D histograms with soft assignment. Specifically, two samples  $x_i, x_j$  from the same person form a positive pair, and the corresponding label is denoted as  $m_{ij} = +1$ . In contrast, two samples from different persons form a negative pair, and the label is denoted as  $m_{ij} = -1$ . Then, we obtain two sample sets  $\mathcal{S}^+ = \{s^+ = \langle \mathcal{F}(x_i), \mathcal{F}(x_j) \rangle | m_{ij} = +1\}$  and  $\mathcal{S}^- = \{s^- = \langle \mathcal{F}(x_i), \mathcal{F}(x_j) \rangle | m_{ij} = -1\}$  corresponding to the similarities of positive and negative pairs, respectively.

Let  $p^+$  and  $p^-$  denote the two probability distributions of  $\mathcal{S}^+$  and  $\mathcal{S}^-$ , respectively. Supposing cosine distance-based methods [5] are used as our baseline, the similarity of each pair is bounded to  $[-1 : 1]$ , which is demonstrated to simplify the task [35]. Motivated by the histogram loss, we estimate this type of one-dimensional distribution by fitting simple histograms with uniformly spaced bins. We adopt  $R$ -dimensional histograms  $H^+$  and  $H^-$ , with the nodes  $t_1 = -1, t_2, \dots, t_R = 1$  uniformly filling  $[-1 : 1]$  with the step  $\Delta = \frac{2}{R-1}$ . Then, we estimate the value  $h_r^+$  of the histogram  $H^+$  at each bin as:

$$h_r^+ = \frac{1}{|\mathcal{S}^+|} \sum_{(i,j): m_{ij}=+1} \delta_{i,j,r}, \quad (3)$$

where  $(i, j)$  spans all the positive pairs. Different from [35], the weights  $\delta_{i,j,r}$  are chosen by an exponential function as:

$$\delta_{i,j,r} = \exp(-\gamma(s_{ij} - t_r)^2), \quad (4)$$

where  $\gamma$  denotes the spread parameter of Gaussian kernel function, and  $t_r$  denotes the  $r$ th node of histograms. We adopt the Gaussian kernel function because it is the most commonly used kernel function for density estimation and robust to the small sample size. The estimation of  $H^-$  proceeds analogously.

### 3.3. Distribution Distillation Loss

We make use of SOTA face recognition engines like [5], to obtain the similarity distributions from two kinds of samples: easy and hard samples. Here, easy samples indicate that the FR engine performs well, in which the similarity

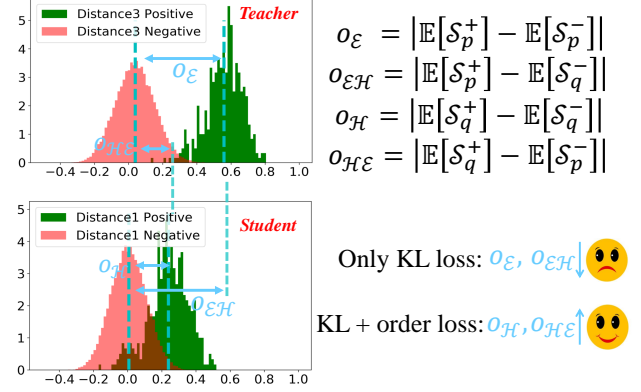


Figure 3: **Illustration on the effects of our order loss.** Left: Similarity distributions constructed by Arcface [5] on dataset SC-face, in which we have 4 kinds of order distances formed from both of the teacher and student distributions according to Eq. 6.

distributions of positive and negative pairs are clearly separated (see the teacher distribution in Fig. 3), while hard samples indicate that the FR engine performs poorly, in which the similarity distributions may be highly overlapped (see the student distribution in Fig. 3).

**KL Divergence Loss.** To narrow the performance gap between the easy and hard samples, we constrain the similarity distribution of hard samples (*i.e.*, student distribution) to approximate the similarity distribution of easy samples (*i.e.*, teacher distribution). The teacher distribution consists of two similarity distributions of both positive and negative pairs, denoted as  $P^+$  and  $P^-$ , respectively. Similarly, the student distribution also consists of two similarity distributions, denoted as  $Q^+$  and  $Q^-$ . Motivated by the previous KD methods [11, 56], we adopt the KL divergence to constrain the similarity between the student and teacher distributions, which is defined as follows:

$$\begin{aligned} \mathcal{L}_{KL} &= \lambda_1 \mathbb{D}_{KL}(P^+ || Q^+) + \lambda_2 \mathbb{D}_{KL}(P^- || Q^-) \\ &= \underbrace{\lambda_1 \sum_s P^+(s) \log \frac{P^+(s)}{Q^+(s)}}_{KL \text{ loss on pos. pairs}} + \underbrace{\lambda_2 \sum_s P^-(s) \log \frac{P^-(s)}{Q^-(s)}}_{KL \text{ loss on neg. pairs}}, \end{aligned} \quad (5)$$

where  $\lambda_1, \lambda_2$  are the weight parameters.

**Order Loss.** However, only performing KL loss does not guarantee satisfying performance. In fact, the teacher distribution may choose to approach the student distribution and lead to more confusion regions between the distributions of positive and negative pairs, which is opposite to our objective (See Fig. 3). To address this problem, we design a simple yet effective term named *order loss*, which minimizes the distances between the expectations of similarity distributions from the negative and positive pairs to control the overlap. Our order loss can be formulated as follows:

$$\mathcal{L}_{order} = -\lambda_3 \sum_{(i,j) \in (p,q)} (\mathbb{E}[S_i^+] - \mathbb{E}[S_j^-]), \quad (6)$$



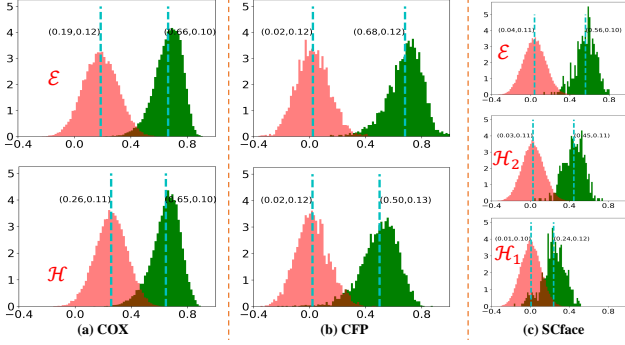


Figure 4: **Illustrations on similarity distribution differences** between easy and hard samples on various variations, including race on COX, pose on CFP, and resolution on SCface respectively. (·, ·) indicates the mean and standard deviation of the distribution.

where  $S_p^+$  and  $S_p^-$  denote the similarities of positive and negative pairs of the teacher distribution;  $S_q^+$  and  $S_q^-$  denote the similarities of positive and negative pairs of the student distribution; and  $\lambda_3$  is the weight parameter.

In summary, the entire formulation of our distribution distillation loss is:  $\mathcal{L}_{DDL} = \mathcal{L}_{KL} + \mathcal{L}_{order}$ . DDL can be easily extended to multiple student distributions as follows:

$$\mathcal{L}_{DDL} = \sum_{i=1}^K \mathbb{D}_{KL}(P||Q_i) - \lambda_3 \sum_{i,j \in (p, q_1 \dots q_K)} (\mathbb{E}[S_i^+] - \mathbb{E}[S_j^-]), \quad (7)$$

where  $K$  is the number of student distributions. Further, to maintain the performance on easy samples, we incorporate the loss function of Arcface [5], and thus the final loss is:

$$\mathcal{L}(\Theta) = \mathcal{L}_{DDL} + \mathcal{L}_{Arcface}, \quad (8)$$

where  $\Theta$  denotes the parameter set. Note that  $\mathcal{L}_{Arcface}$  can be easily replaced by any kind of popular losses in FR.

### 3.4. Generalization on Various Variations

Next, we discuss the generalization of DDL on various variations, which defines our *application scenarios* and how we select easy/hard samples. Basically, we can distinguish the easy and hard samples according to whether the image contains large facial variations that may hinder the identity information, *e.g.*, low-resolution and large pose variation.

**Observation from Different Variations.** Our method assumes that two or more distributions, each computed from a subset of training data, have differences among themselves, which is a popular phenomenon in face recognition and is demonstrated in Fig. 4. It shows similarity distributions of normal and challenging samples based on Arcface [5] trained by CASIA except CFP, which is trained on VGGFace2. As we can see, 1) since CASIA is biased to Caucasian, Mongolian samples in COX are more difficult and thus relatively regarded as the hard samples, 2) different variations share a common observation that the similarity distributions of challenging samples are usually different

Table 1: **Details on diverse datasets** used in this work.

Datasets	Subjects #	Image #	Variation	Size	Train	Test
SCface [9]	130	4,160	Resolution	Small	✓	✓
COX [12]	1,000	—	Race	Small	✓	✓
CASIA [49]	10,575	494,414	All	Medium	✓	
VGGFace2 [2]	9,131	3.31M	All	Large	✓	
MS1M [5]	85K	5.8M	All	Very Large	✓	
CFP-FP [25]	500	7000	Pose	Small		✓
CPLFW [58]	5749	11652	Pose	Small		✓
IJB-B [43]	1845	76.8K	ALL	Large		✓
IJB-C [20]	3531	148.8K	ALL	Large		✓

from those of easy samples, 3) variations with different extents may have different similarity distributions (*e.g.*,  $\mathcal{H}_1$  and  $\mathcal{H}_2$  in Fig. 4(c)). In summary, when a task satisfies that *the similarity distributions differ between easy and hard samples*, our method is a good solution and one can enjoy the performance improvement by properly constructing the positive and negative pairs, which is validated in Sec. 4.3.

**Performance Balance Between Easy/Hard Samples.** Improving the performance from hard samples while maintaining the performance on easy samples is a trade-off. Two factors in our method help maintain performance on easy samples. On one hand, we incorporate the SOTA ArcFace loss [5] to maintain the feature discriminability on easy samples. On the other hand, our order loss minimizes the distance between the expectations of similarity distributions from the negative and positive pairs, which helps control the overlap between positive and negative pairs.

**Discussions on Mixture Variations.** As in Eq. 7, our method can be easily extended to multiple variations for one task (*e.g.*, low resolution). An alternative is to mix the variations with different extents from one task into *one* student distribution, which, as shown in Sec. 4.2, is not good enough to specifically model the different extents and tends to lead to lower performance. As for different variations from different tasks, one may also construct multiple teacher-student distribution pairs to address the corresponding task respectively, which can be a good future direction.

## 4. Experiments

### 4.1. Implementation Details

**Datasets.** As shown in Tab. 1, we separately employ SCface [9], COX [12], CASIA-WebFace [49], VGGFace2 [2] and the refined MS1M [5] as our training data to conduct fair comparisons with other methods. We extensively test our method on benchmarks with diverse variations, *i.e.*, COX on race, SCface on resolution, CFP and CPLFW on Pose, as well as generic large-scale benchmarks IJB-B and IJB-C. For COX, the data are collected from two races: Caucasian and Mongolian, but no race label is given. We manually label 428 Mongolians and 572 Caucasians to conduct experiments, in which half of both races are used for finetuning and the others for testing. For SCface, following [18], 50 subjects are used for finetuning and 80 sub-

Table 2: **Extensive ablation studies on SCface dataset. All methods are trained on CASIA with a ResNet50 backbone.**  $d_1$ ,  $d_2$  and  $d_3$  indicate images in SCface [9] captured at distances of 4.2, 2.6 and 1.0m, respectively. Each color corresponds to a type of ablation study experimental setting.

	EMD	JS	KL	Order	Random	Hard Mining	Mixture	Specific	Softmax	ArcFace	$d_1$	$d_2$	$d_3$	Avg.
Distance metric	✓			✓		✓		✓		✓	78.0	97.8	96.8	90.5
		✓				✓		✓		✓	83.0	<b>98.3</b>	<b>99.0</b>	93.4
			✓			✓		✓		✓	76.0	94.3	98.5	89.6
				✓		✓		✓		✓	80.8	97.5	<b>99.0</b>	92.4
Mining strategy			✓	✓	✓			✓		✓	80.3	96.3	95.3	90.6
Specific training			✓	✓			✓			✓	81.5	97.0	97.8	92.1
Loss									✓		77.3	97.5	97.8	90.8
									✓	✓	67.3	93.5	98.0	86.3
DDL (ours)			✓	✓		✓		✓			<b>90.0</b>	98.0	97.5	<b>95.2</b>
			✓	✓		✓		✓		✓	86.8	<b>98.3</b>	98.3	94.4

jects are for testing. In the testing stage, we conduct face identification, where HR image is used as the gallery and LR images with three different resolutions form the probe. Specifically, the LR images are captured at three distances: 4.2m for  $d_1$ , 2.6m for  $d_2$  and 1.0m for  $d_3$ .

**Training Setting.** We follow [5, 38] to generate the normalised faces ( $112 \times 112$ ) with five landmarks [54]. For the embedding network, we adopt ResNet50 and ResNet100 as in [5]. Our work is implemented in Tensorflow [7]. We train models on 8 NVIDIA Tesla P40 GPUs. On SCface, we set the number of positive/negative pairs as  $b = 16$ , thus the batch size on one GPU is  $3b \times 3 = 96$ , including one teacher distribution and two student distributions (see Fig. 4(c)). On other datasets, we set  $b$  to 32, thus the batch size per GPU is  $3b \times 2 = 192$ . The numbers of iterations are 1K, 2K and 20K on SCface, COX and VGGFace2, respectively. The models are trained with SGD, with momentum 0.9 and weight decay  $5e^{-4}$ . The learning rate is  $1e^{-3}$ , and is divided by 10 at half of iterations. All the weight parameter are consistent across all the experiments.  $\lambda_1$ ,  $\lambda_2$  and  $\lambda_3$  equal to  $1e^{-1}$ ,  $2e^{-2}$ ,  $5e^{-1}$ , respectively.

## 4.2. Ablation Study

**Effects of Distance Metric on Distributions.** We investigate the effects of several commonly used distribution metrics to constrain the teacher and student distributions in our DDL, including KL divergence, Jensen-Shannon (JS) divergence, and Earth Mover Distance (EMD). Although KL divergence does not qualify as a statistical metric, it is widely used as a measure of how one distribution is different from another. JS divergence is a symmetric version of KL divergence. EMD is another distance function between distributions on a given metric space and has seen success in image synthesis [8]. We incorporate our order loss with the above distance metrics, and report the results in Tab. 2. As we can see, we choose the KL divergence in our DDL since it achieves the best performance, which shares similar conclusion in [56]. To further investigate the effectiveness of each component in our loss, we train the network with each com-

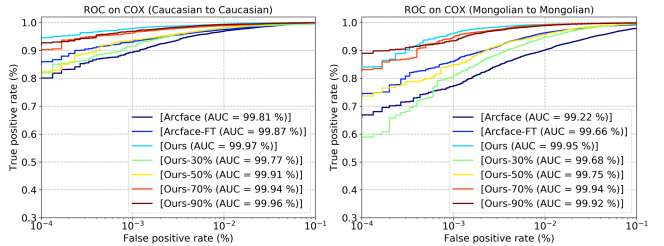


Figure 5: **Effects of Number of Training Subjects on COX datasets.** Compared to Arcface-FT, our method can achieve comparable results with only *half* of the entire training subjects.

ponent, respectively. As shown in Tab. 2, only KL or only Order does not guarantee satisfying performance, while using both components leads to better results.

**Effects of Random vs. Hard Mining.** To investigate the effect of hard sample mining in our method, we train models on SCface with the corresponding strategy (*i.e.*, negative pairs with the largest similarity are selected), and without the strategy by randomly selecting the negative pairs, respectively. The comparative results are reported in Tab. 2. Comparing the results of “Random” selecting, it is clear that our hard mining version outperforms the one without.

**Effects of Mixture vs. Specific training.** As mentioned in Sec. 3.4, we basically construct different student distributions for samples with different extents of variations on SCface. Here, we mix two variations from  $d_1$  and  $d_2$  into *one* student distribution. The comparison between our specific and mixture training is also shown in Tab. 2. As we expected, the mixture version is worse than the specific version, but is still better than the conventional finetuning (*i.e.*, Avg. being 86.3), which indicates that properly constructing different hard samples for the target tasks may maximize the advantages of our method.

**Effects of Equipping DDL with Different Losses.** Next, we conduct experiment to investigate the effects of equipping our DDL with different losses. We choose the softmax and Arcface as our baselines, and perform conventional

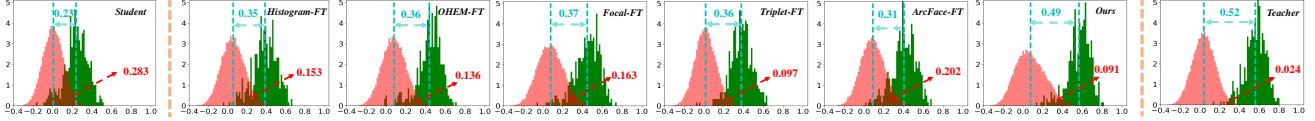


Figure 6: **Illustrations on similarity distributions of different SOTA methods**, which are all pre-trained by CASIA with ResNet50 and then finetuned on SCface. The leftmost and rightmost are the student and teacher distributions estimated from a pre-trained ArcFace model on  $d_1$  and  $d_3$  settings, respectively. The similarity distributions in the middle are obtained by various methods finetuned on SCface. The red number indicates the *histogram intersection* between the estimated similarity distributions from the positive and negative pairs.

finetuning for them on SCface. As show in Tab. 2, our DDL consistently outperforms the conventional finetuning on the target test sets. Also, it is surprising that the softmax versions are consistently better than the Arcface ones on SCface. The reason may be that Arcface is prone to overfitting when fine-tuned on such small dataset.

**Effects of Number of Training Subjects.** Here, we conduct tests on COX dataset to show the effects on using different numbers of training subjects. Specifically, we adopt 10%, 30%, 50%, 70%, 90% and 100% of training subjects, respectively. A pre-trained Arcface on CASIA is used as the baseline. For fair comparison, we also compare our method against Arcface with conventional finetuning (*i.e.*, Arcface-FT). From Fig. 5 we see that: 1) Compared to Arcface-FT, our method clearly boosts the performance on Caucasian-Caucasian and Mongolian-Mongolian verification tests with comparable training data. 2) Our method can achieve comparable performance with only *half* of the training data.

### 4.3. Comparisons with SOTA Methods

**Resolution on SCface.** SCface defines face identification with HR and LR faces. It mimics the real-world surveillance watch-list problem, where the gallery contains HR faces and the probe consists of LR faces captured from surveillance cameras. We compare our method with SOTA low-resolution face recognition methods in Tab. 3. Most results are directly cited from [18], while the results of Arcface comes from our re-implementation. Based on Tab. 3, we have some observations: 1) The baseline Arcface model achieves much better results than the other methods without finetuning, especially on those relative high-resolution images from  $d_3$ . 2) Our (CASIA+ResNet50)-FT version already outperforms all of the other methods, including Arcface (MS1M+ResNet100)-FT, which uses a larger model that is trained by a much larger dataset (10× more as in Tab. 1). 3) We achieve significant improvement on  $d_1$  setting, which is the hardest. This demonstrates the effectiveness of our novel loss. 4) Our method consistently outperforms the conventional finetuning on different backbones trained by different datasets, which also demonstrates our generalization ability. 5) Histogram loss performs poorly, which demonstrates the effects of our constrain between teacher and student distributions.

Table 3: **Rank-1 performance (%) of face identification on SCface testing set.** ‘-FT’ represents finetuning with SCface training set. The results are cited from [18] except ArcFace. ‘CASIA+R50’ denotes ResNet50 pre-trained with CASIA.

Distance →	$d_1$	$d_2$	$d_3$	avg.
LDMS [48]	62.7	70.7	65.5	66.3
RICNN [52]	23.0	66.0	74.0	54.3
LightCNN [44]	35.8	79.0	93.8	69.5
Center Loss [42]	36.3	81.8	94.3	70.8
ArcFace (CASIA+R50)	48.0	92.0	99.3	79.8
ArcFace (MS1M+R100)	58.9	98.3	<b>99.5</b>	85.5
LightCNN-FT	49.0	83.8	93.5	75.4
Center Loss-FT	54.8	86.3	95.8	79.0
DCR-FT [18]	73.3	93.5	98.0	88.3
Histogram (CASIA+R50)-FT [35]	74.3	95.0	97.3	88.8
OHEM (CASIA+R50)-FT [27]	82.5	97.3	97.5	92.7
Focal (CASIA+R50)-FT [15]	76.8	95.5	96.8	89.7
Triplet (CASIA+R50)-FT [5]	84.2	97.2	99.2	93.5
ArcFace (CASIA+R50)-FT	67.3	93.5	98.0	86.3
ArcFace (MS1M+R100)-FT	80.5	98.0	99.5	92.7
<b>Ours (CASIA+R50)</b>	86.8	98.3	98.3	94.4
<b>Ours (MS1M+R100)</b>	<b>93.2</b>	<b>99.2</b>	98.5	<b>97.0</b>

Finally, different to the prior hard mining methods where the hard samples are mined based on the loss values during the training process (*i.e.*, Triplet loss [24], Focal loss [15] and OHEM [27]), we *pre-define* hard samples according to human prior. Penalizing *individual* sample or triplet in the previous hard mining methods does not leverage sufficient contextual insight of overall distribution. While DDL minimizes the difference of *global* similarity distributions between the easy and hard samples, which is more robust for tackling hard samples and against the noisy samples.

Fig. 6 illustrates the estimated similarity distributions of various SOTA methods. To quantify the difference among these methods, we introduce two statistics for evaluation, the expectation margin and histogram intersection (*i.e.*,  $\sum_{r=1}^R \min(h_r^+, h_r^-)$ ) between the two distributions from positive and negative pairs. Typically, smaller histogram intersection and larger expectation margin indicate better verification/identification performance, since it means that more discriminative deep embeddings are learned [35]. As we can see, our DDL achieves the closest statistics as the teacher distribution, and thus obtains the best performance.

**Pose on CFP-FP and CPLFW.** We compare our method with SOTA pose-invariant methods [1, 4, 22, 34, 50] and generic solutions [2, 5, 16, 39, 40, 42]. Since VGGFace2 in-

Table 4: **Verification comparison with SOTA methods** on LFW and two popular pose benchmarks: CFP-FP and CPLFW.

Methods (%)	LFW	CFP-FP	CPLFW
HUMAN-Individual	97.27	94.57	81.21
HUMAN-Fusion	99.85	—	85.24
Triplet Loss (CVPR'15)	98.98	91.90	—
Center Loss (ECCV'16) [42]	98.75	—	77.48
SphereFace (CVPR'17) [16]	99.27	—	81.40
DRGAN (CVPR'17) [34]	—	93.41	—
Peng <i>et al.</i> (ICCV'17) [22]	—	93.76	—
Yin <i>et al.</i> (TIP'17) [50]	98.27	94.39	—
VGGFace2 (FG'18) [2]	99.43	—	84.00
Dream (CVPR'18) [1]	—	93.98	—
Deng <i>et al.</i> (CVPR'18) [4]	99.60	94.05	—
SV-Arc-Softmax (arXiv'19) [40]	99.78	98.28	92.83
CO-Mining (ICCV'19) [39]	—	95.87	87.31
ArcFace (MS1M+R100)-Official [5] <sup>1</sup>	<b>99.82</b>	98.37	92.08
ArcFace (MS1M+R100)	99.80	98.29	92.52
ArcFace (VGG+R100)	99.62	98.30	93.13
<b>Ours (VGG+R100)</b>	99.68	<b>98.53</b>	<b>93.43</b>

cludes comprehensive pose variations, we use it to pre-train a ResNet100 with ArcFace. Next, we estimate the pose of each image [23] in VGGFace2, and construct teacher (yaw  $< 10^\circ$ ) and student distributions (yaw  $> 45^\circ$ ), to finetune the model with our loss. From Tab. 4, we can see that: 1) Our Arcface re-implementations achieve comparable results against the official version, with similar results on LFW and CFP-FP, as well as better performance on CPLFW. ArcFace is also much better than other methods, including those pose-invariant face recognition methods. 2) Our method achieves the best performance on both pose benchmarks, which meanwhile maintains the performance on LFW (*i.e.*, 99.68% vs. 99.62%).

Note that when using the model pre-trained on MS1M, and finetuning it with easy/hard samples from VGGFace2, our method can further push the performance to a higher level (**99.06%** on CFP-FP and **94.20%** on CPLFW), which is the *first* method that exceeds 99.0% on CFP-FP and 94.0% on CPLFW using cropped images by MTCNN. Besides, we also train our DDL on the smaller training set CASIA with a smaller backbone ResNet50. Again, our DDL outperforms the SOTA methods. Please refer to our supplementary material for detailed results.

**Large-Scale Benchmarks: IJB-B and IJB-C.** On the IJB-B and IJB-C datasets, we employ VGGFace2 with ResNet50 for a fair comparison with recent methods. We first construct the teacher and student distributions according to the pose of each image, and then follow the testing protocol in [5] to take the *average of the image features* as the corresponding template representation without bells and whistles. Tab. 5 and Tab. 6 show the 1:1 verification and 1:N identification comparisons with the recent SOTA meth-

<sup>1</sup>Results are from the official ResNet100 pre-trained with MS1M: <https://github.com/deepinsight/insightface>.

Table 5: **1:1 verification TAR** on the IJB-B and IJB-C datasets. All methods are trained on VGGFace2 with ResNet50.

Methods (%)	IJB-B			IJB-C		
	FAR=1e-5	1e-4	1e-3	FAR=1e-5	1e-4	1e-3
VGGFace2 [2]	67.1	80.0	88.7	74.7	84.1	90.9
MN [46]	70.8	83.1	90.9	77.1	86.2	92.7
DCN [45]	—	84.9	93.7	—	88.5	94.7
ArcFace [5]	80.5	89.9	94.5	86.1	92.1	96.0
<b>Ours</b>	<b>83.4</b>	<b>90.7</b>	<b>95.2</b>	<b>88.4</b>	<b>93.1</b>	<b>96.3</b>

Table 6: **1:N (mixed media) Identification** on IJB-B/C. All methods are trained on VGGFace2 with ResNet50. VGGFace2 is cited from paper, and ArcFace is from its official released model.

Methods (%)	IJB-B				IJB-C			
	FPIR=0.01	FPIR=0.1	Rank 1	Rank 5	FPIR=0.01	FPIR=0.1	Rank 1	Rank 5
VGGFace2 [2]	70.6	83.9	90.1	94.5	74.6	84.2	91.2	94.9
ArcFace [5]	73.1	88.2	93.6	96.5	79.6	89.5	94.8	96.9
<b>Ours</b>	<b>76.3</b>	<b>89.5</b>	<b>93.9</b>	<b>96.6</b>	<b>85.4</b>	<b>91.1</b>	<b>95.4</b>	<b>97.2</b>

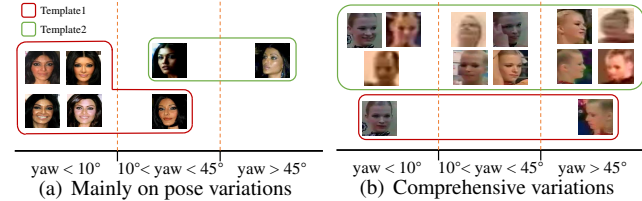


Figure 7: **Examples of positive template pairs classified correctly by ours while ArcFace fails** at FAR=1e-5 from IJB-B.

ods, respectively. Note that our method is *not* a set-based face recognition method, and the experiments on these two datasets are just to prove that our DDL can obtain more discriminant features than the generic method like ArcFace, even on all-variations-included datasets.

Fig. 7 illustrates two examples of positive template pairs that are classified correctly by ours but ArcFace fails. Benefiting from the distribution constraint on pose variation, our DDL learns more *discriminant pose-invariant features*, and thus leading to better performance on templates that differs on poses (Fig. 7(a)). Interestingly, when comprehensive variations exist, *e.g.*, resolution (Fig. 7(b)), ArcFace again fails while our method shows robustness to some extent.

**Time Complexity.** Compared with conventional finetuning, the only additional operation in our training is to construct the positive and negative pairs in each mini-batch. The positive pairs are constructed offline, and thus has little influence on the training speed. For negative pairs, since we adopt online hard sample mining to grab the hardest  $b$  pairs from the total  $b \times (b - 1)/2$  negative pairs for each distribution, our training step is slightly slower than conventional finetuning, which is still fast. Specifically, with the same environment, conventional finetuning on COX dataset costs 39 minutes for training, while ours costs 43 minutes. Hence, our DDL only has small effects on the training pro-



cess, which totally has **NO** influence for inference.

## 5. Conclusion

In this paper, we propose a novel *general* framework, named Distribution Distillation Loss (DDL), aiming to improve various variation-*specific* tasks, which comes from the observations that state-of-the-art methods (*e.g.*, Arcface) witness significant performance gap between easy and hard samples. The key idea of our method is to construct a teacher and a student distribution from easy and hard samples, respectively. Then, the proposed loss drives the student distribution to approximate the teacher distribution to reduce the overlap between the positive and negative pairs. Extensive experiments demonstrate the effectiveness of our DDL on a wide range of recognition tasks compared to the state-of-the-art face recognition methods.

## References

- [1] Kaidi Cao, Yu Rong, Cheng Li, Xiaoou Tang, and Chen Change Loy. Pose-robust face recognition via deep residual equivariant mapping. In *CVPR*, pages 5187–5196, 2018. 7, 8
- [2] Qiong Cao, Li Shen, Weidi Xie, Omkar M Parkhi, and Andrew Zisserman. Vggface2: A dataset for recognising faces across pose and age. In *FG*, pages 67–74. IEEE, 2018. 5, 7, 8
- [3] Yu Chen, Ying Tai, Xiaoming Liu, Chunhua Shen, and Jian Yang. Fsnet: End-to-end learning face super-resolution with facial priors. In *CVPR*, pages 2492–2501, 2018. 2, 3
- [4] Jiankang Deng, Shiyang Cheng, Niannan Xue, Yuxiang Zhou, and Stefanos Zafeiriou. Uv-gan: Adversarial facial uv map completion for pose-invariant face recognition. In *CVPR*, pages 7093–7102, 2018. 7, 8
- [5] Jiankang Deng, Jia Guo, Niannan Xue, and Stefanos Zafeiriou. Arcface: Additive angular margin loss for deep face recognition. In *CVPR*, pages 4690–4699, 2019. 1, 2, 3, 4, 5, 6, 7, 8
- [6] Jiankang Deng, Yuxiang Zhou, and Stefanos Zafeiriou. Marginal loss for deep face recognition. In *CVPR Workshops*, pages 60–68, 2017. 2
- [7] Martín Abadi et al. TensorFlow: Large-scale machine learning on heterogeneous systems, 2015. Software available from tensorflow.org. 6
- [8] Ian Goodfellow, Jean Pouget-Abadie, Mehdi Mirza, Bing Xu, David Warde-Farley, Sherjil Ozair, Aaron Courville, and Yoshua Bengio. Generative adversarial nets. In *NIPS*, pages 2672–2680, 2014. 3, 6
- [9] Mislav Grgic, Kresimir Delac, and Sonja Grgic. Sface—surveillance cameras face database. *Multimedia Tools and Applications*, 51(3):863–879, 2011. 1, 2, 5, 6
- [10] Pablo H Hennings-Yeomans, Simon Baker, and BVK Vijaya Kumar. Simultaneous super-resolution and feature extraction for recognition of low-resolution faces. In *CVPR*, pages 1–8. IEEE, 2008. 3
- [11] Geoffrey Hinton, Oriol Vinyals, and Jeff Dean. Distilling the knowledge in a neural network. In *NIPS Workshop*, 2014. 3, 4
- [12] Zhiwu Huang, Shiguang Shan, Ruiping Wang, Haihong Zhang, Shihong Lao, Alifu Kuerban, and Xilin Chen. A benchmark and comparative study of video-based face recognition on cox face database. *IEEE Transactions on Image Processing*, 24(12):5967–5981, 2015. 5
- [13] Zehao Huang and Naiyan Wang. Like what you like: Knowledge distill via neuron selectivity transfer. *arXiv:1707.01219v2*, 2017. 3
- [14] Zhen Lei, Timo Ahonen, Matti Pietikäinen, and Stan Z Li. Local frequency descriptor for low-resolution face recognition. In *FG*, pages 161–166. IEEE, 2011. 2
- [15] Tsung-Yi Lin, Priya Goyal, Ross Girshick, Kaiming He, and Piotr Dollár. Focal loss for dense object detection. In *ICCV*, pages 2980–2988, 2017. 7
- [16] Weiyang Liu, Yandong Wen, Zhiding Yu, Ming Li, Bhiksha Raj, and Le Song. Sphreface: Deep hypersphere embedding for face recognition. In *CVPR*, pages 212–220, 2017. 2, 7, 8
- [17] Weiyang Liu, Yandong Wen, Zhiding Yu, and Meng Yang. Large-margin softmax loss for convolutional neural networks. In *ICML*, volume 2, page 7, 2016. 2
- [18] Ze Lu, Xudong Jiang, and Alex Kot. Deep coupled resnet for low-resolution face recognition. *IEEE Signal Processing Letters*, 25(4):526–530, 2018. 3, 5, 7
- [19] Laurens van der Maaten and Geoffrey Hinton. Visualizing data using t-sne. *Journal of Machine Learning Research*, 9(Nov):2579–2605, 2008. 1
- [20] Brianna Maze, Jocelyn Adams, James A Duncan, Nathan Kalka, Tim Miller, Charles Otto, Anil K Jain, W Tyler Niggel, Janet Anderson, Jordan Cheney, et al. Iarpa janus benchmark-c: Face dataset and protocol. In *ICB*, pages 158–165. IEEE, 2018. 2, 5
- [21] Omkar M Parkhi, Andrea Vedaldi, Andrew Zisserman, et al. Deep face recognition. In *BMVC*, volume 1, page 6, 2015. 2
- [22] Xi Peng, Xiang Yu, Kihyuk Sohn, Dimitris N Metaxas, and Manmohan Chandraker. Reconstruction-based disentanglement for pose-invariant face recognition. In *ICCV*, pages 1623–1632, 2017. 7, 8
- [23] Nataniel Ruiz, Eunji Chong, and James M Rehg. Fine-grained head pose estimation without keypoints. In *CVPR Workshops*, pages 2074–2083, 2018. 8
- [24] Florian Schroff, Dmitry Kalenichenko, and James Philbin. Facenet: A unified embedding for face recognition and clustering. In *CVPR*, pages 815–823, 2015. 2, 7
- [25] Soumyadip Sengupta, Jun-Cheng Chen, Carlos Castillo, Vishal M Patel, Rama Chellappa, and David W Jacobs. Frontal to profile face verification in the wild. In *WACV*, pages 1–9. IEEE, 2016. 5
- [26] Sumit Shekhar, Vishal M Patel, and Rama Chellappa. Synthesis-based recognition of low resolution faces. In *IJCB*, pages 1–6. IEEE, 2011. 2
- [27] Abhinav Shrivastava, Abhinav Gupta, and Ross Girshick. Training region-based object detectors with online hard example mining. In *CVPR*, pages 761–769, 2016. 7

- [28] Yi Sun, Yuheng Chen, Xiaogang Wang, and Xiaoou Tang. Deep learning face representation by joint identification-verification. In *NIPS*, pages 1988–1996, 2014. 2
- [29] Yi Sun, Xiaogang Wang, and Xiaoou Tang. Deep learning face representation from predicting 10,000 classes. In *CVPR*, pages 1891–1898, 2014. 2
- [30] Ying Tai, Jian Yang, and Xiaoming Liu. Image super-resolution via deep recursive residual network. In *CVPR*, pages 3147–3155, 2017. 3
- [31] Ying Tai, Jian Yang, Xiaoming Liu, and Chunyan Xu. Memnet: A persistent memory network for image restoration. In *ICCV*, pages 4539–4547, 2017. 3
- [32] Ying Tai, Jian Yang, Yigong Zhang, Lei Luo, Jianjun Qian, and Yu Chen. Face recognition with pose variations and misalignment via orthogonal procrustes regression. *IEEE Transactions on Image Processing*, 25(6):2673–2683, 2016. 2, 3
- [33] Yaniv Taigman, Ming Yang, Marc’Aurelio Ranzato, and Lior Wolf. Deepface: Closing the gap to human-level performance in face verification. In *CVPR*, pages 1701–1708, 2014. 2
- [34] Luan Tran, Xi Yin, and Xiaoming Liu. Disentangled representation learning gan for pose-invariant face recognition. In *CVPR*, pages 1415–1424, 2017. 2, 3, 7, 8
- [35] Evgeniya Ustinova and Victor Lempitsky. Learning deep embeddings with histogram loss. In *NIPS*, pages 4170–4178, 2016. 2, 4, 7
- [36] Feng Wang, Jian Cheng, Weiyang Liu, and Haijun Liu. Additive margin softmax for face verification. *IEEE Signal Processing Letters*, 25(7):926–930, 2018. 2
- [37] Feng Wang, Xiang Xiang, Jian Cheng, and Alan Loddon Yuille. Normface: 12 hypersphere embedding for face verification. In *ACMMM*, pages 1041–1049. ACM, 2017. 2
- [38] Hao Wang, Yitong Wang, Zheng Zhou, Xing Ji, Dihong Gong, Jingchao Zhou, Zhifeng Li, and Wei Liu. Cosface: Large margin cosine loss for deep face recognition. In *CVPR*, pages 5265–5274, 2018. 2, 6
- [39] Xiaobo Wang, Shuo Wang, Jun Wang, Hailin Shi, and Tao Mei. Co-mining: Deep face recognition with noisy labels. In *ICCV*, pages 9358–9367, 2019. 7, 8
- [40] Xiaobo Wang, Shuo Wang, Shifeng Zhang, Tianyu Fu, Hailin Shi, and Tao Mei. Support vector guided softmax loss for face recognition. *arXiv:1812.11317*, 2018. 7, 8
- [41] Xiaojie Wang, Rui Zhang, Yu Sun, and Jianzhong Qi. Kdgan: knowledge distillation with generative adversarial networks. In *NIPS*, pages 775–786, 2018. 3
- [42] Yandong Wen, Kaipeng Zhang, Zhifeng Li, and Yu Qiao. A discriminative feature learning approach for deep face recognition. In *ECCV*, pages 499–515. Springer, 2016. 2, 7, 8
- [43] Cameron Whitelam, Emma Taborsky, Austin Blanton, Brianna Maze, Jocelyn Adams, Tim Miller, Nathan Kalka, Anil K Jain, James A Duncan, Kristen Allen, et al. Iarpa janus benchmark-b face dataset. In *CVPR Workshops*, pages 90–98, 2017. 2, 5
- [44] Xiang Wu, Ran He, Zhenan Sun, and Tieniu Tan. A light cnn for deep face representation with noisy labels. *IEEE Transactions on Information Forensics and Security*, 13(11):2884–2896, 2018. 7
- [45] Weidi Xie, Li Shen, and Andrew Zisserman. Comparator networks. In *ECCV*, pages 782–797, 2018. 8
- [46] Weidi Xie and Andrew Zisserman. Multicolumn networks for face recognition. In *BMVC*, 2018. 8
- [47] Zheng Xu, Yen-Chang Hsu, and Jiawei Huang. Training shallow and thin networks for acceleration via knowledge distillation with conditional adversarial networks. *arXiv:1709.00513v2*, 2018. 3
- [48] Fuwei Yang, Wenming Yang, Riqiang Gao, and Qingmin Liao. Discriminative multidimensional scaling for low-resolution face recognition. *IEEE Signal Processing Letters*, 25(3):388–392, 2017. 7
- [49] Dong Yi, Zhen Lei, Shengcai Liao, and Stan Z Li. Learning face representation from scratch. *arXiv:1411.7923*, 2014. 5
- [50] Xi Yin and Xiaoming Liu. Multi-task convolutional neural network for pose-invariant face recognition. *IEEE Transactions on Image Processing*, 27(2):964–975, 2017. 3, 7, 8
- [51] Xi Yin, Xiang Yu, Kihyuk Sohn, Xiaoming Liu, and Manmohan Chandraker. Towards large-pose face frontalization in the wild. In *ICCV*, pages 3990–3999, 2017. 2
- [52] Dan Zeng, Hu Chen, and Qijun Zhao. Towards resolution invariant face recognition in uncontrolled scenarios. In *ICB*, pages 1–8. IEEE, 2016. 7
- [53] Kaipeng Zhang, Zhanpeng Zhang, Chia-Wen Cheng, Winston H Hsu, Yu Qiao, Wei Liu, and Tong Zhang. Super-identity convolutional neural network for face hallucination. In *ECCV*, pages 183–198, 2018. 2, 3
- [54] Kaipeng Zhang, Zhanpeng Zhang, Zhifeng Li, and Yu Qiao. Joint face detection and alignment using multitask cascaded convolutional networks. *IEEE Signal Processing Letters*, 23(10):1499–1503, 2016. 6
- [55] Xiao Zhang, Zhiyuan Fang, Yandong Wen, Zhifeng Li, and Yu Qiao. Range loss for deep face recognition with long-tailed training data. In *ICCV*, pages 5409–5418, 2017. 2
- [56] Ying Zhang, Tao Xiang, Timothy M Hospedales, and Huchuan Lu. Deep mutual learning. In *CVPR*, pages 4320–4328, 2018. 3, 4, 6
- [57] Jian Zhao, Lin Xiong, Yu Cheng, Yi Cheng, Jianshu Li, Li Zhou, Yan Xu, Jayashree Karlekar, Sugiri Pranata, Shengmei Shen, et al. 3d-aided deep pose-invariant face recognition. In *IJCAI*, volume 2, page 11, 2018. 3
- [58] Tianyue Zheng and Weihong Deng. Cross-pose lfw: A database for studying crosspose face recognition in unconstrained environments. *Beijing University of Posts and Telecommunications, Tech. Rep*, pages 18–01, 2018. 2, 5
- [59] Wilman WW Zou and Pong C Yuen. Very low resolution face recognition problem. *IEEE Transactions on Image Processing*, 21(1):327–340, 2011. 3